Chapter 7

Visualizing Phase Separation and Shape Deformation in Giant Unilamellar Vesicles (GUVs) using Fluorescence Microscopy

7.1 Introduction

As discussed in chapter 1, studies on giant unilamellar vesicles (GUVs) made from artificial membranes have received a lot of attention since they are excellent model systems for biological membranes. There have been a large number of studies of the influence of cholesterol on lipid membranes using fluorescence microscopy of GUVs. In earlier chapters, we have presented the phase behaviour and structure of lipid–cholesterol membranes obtained from x-ray diffraction studies. These experiments were carried out with multilamellar stack of bilayers. The present chapter describes confocal fluorescence microscopy studies on GUVs, which were performed in order to obtain complementary information from these systems. Earlier microscopy studies mainly on GUVs are summarized in section 7.2. The experimental details are presented in section 7.3. Finally we discuss our results on GUVs made up of both binary and ternary lipid–cholesterol mixtures in section 7.4.

7.2 Earlier studies

We have already discussed a variety of experimental techniques used to study various physical properties and phase behaviour of lipid–cholesterol membranes in earlier chapters. Here, we will briefly discuss earlier microscopy studies on GUVs composed of lipid–cholesterol mixtures. Fluorescence microscopy studies on GUVs made up of binary lipid–cholesterol mixtures do not exhibit phase separation. However, binary lipid mixtures, such as DPPC/DOPC and DPPC/DLPC, show coexistence of gel and fluid phases below the chain melting transition temperature (T_m) of DPPC [1, 2]. Shape deformations of GUVs made from single component lipid and binary lipid mixtures have been observed near the main transition [1, 3]. These shape transformations have been explained theoretically using membrane elasticity models with various levels of sophistication [4, 5]. Stationary shapes of vesicles were obtained from these models by minimizing the free energy subject to the constraints that the volume and surface area remain constant [5]. These models were also used to explain various shapes observed in DMPC GUVs on changing the temperature [3].

As discussed in chapter 6, GUVs made up of ternary mixtures of a lipid with saturated hydrocarbon chains, a lipid with unsaturated chains and cholesterol show fluid domains, indicating the coexistence of two fluid phases, known as liquid ordered (l_o) and liquid disordered (l_d) [2, 6]. Two-photon fluorescence microscopy on these mixtures also show the coexistence of such domains [7]. These fluid domains were further characterized using fluorescence correlation spectroscopy (FCS) [8]. Diffusion coefficient of the l_o and l_d phases were found to be 2.5×10^{-8} and 5.2×10^{-8} cm^2/s, respectively, indicating much slower lateral diffusion of lipid molecules in the l_o phase. Two-photon microscopy on GUVs made from ternary mixtures of sphingomyelin, DOPC and cholesterol suggests smaller bending rigidity (κ) of the l_d phase compared to the l_o phase [6]. In this study, domains of both l_o and l_d phases were observed to form buds, suggesting that the line tension at the boundary between these two phases is the key factor in the formation of the bud and in determining its size. Recent simulations have also shown the coalescence of the domains to form buds [9].

(a) Rhodamine DHPE   (b) Laurdan
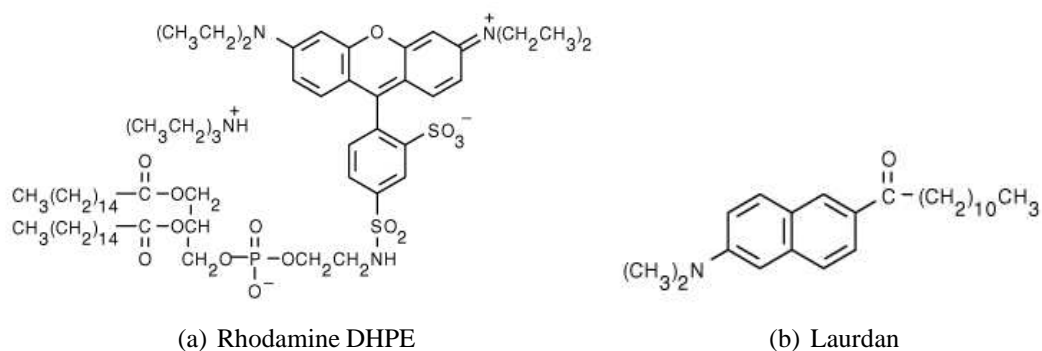
Figure 7.1: Chemical structure of Rhodamine DHPE (a) and Laurdan (b)

7.3   Experimental details

GUVs were prepared using electroformation, first described by Angelova et al. [10]. Details of the technique have been given in chapter 2. GUVs were labeled with Rhodamine DHPE (Rho PE) (Fig. 7.1 a) and Laurdan (Fig. 7.1 b). 0.2 mol% of Rho PE and 0.5 mol% Laurdan were used. Most of the experiments were done at room temperature (23°C). Laurdan is an environment sensitive fluorescence probe and is used widely to determine the lipid phase of the membranes [11]. Laurdan excitation and emission spectra are extremely sensitive to the local environments like solvent polarity and the phase state of lipids [1, 12, 13, 14]. For example, Laurdan molecules dispersed in an apolar solvent show a blue emission (440 nm), but the spectrum gets red shifted when Laurdan is embedded in a polar solvent. The relaxation time of water molecules matches the life-time of Laurdan fluorescence emission. Therefore, during excitation of Laurdan, polar solvent molecules (water) reorient themselves around Laurdan molecules and a part of the excitation energy is spent in reorienting the water molecules, resulting in a red shift of the emission spectrum. When Laurdan is in the membrane, its emission spectrum also depends upon the phase state of the lipid. In the gel phase, Laurdan shows a blue emission (440 nm) , but the emission spectrum shifts to 490 nm (red shifted) when the membrane undergoes a transition to the fluid phase. The amount of water penetrating into the membranes determines the extent of the red shift. Since in the fluid phase water can penetrate more into the membranes, the spectrum is red shifted compared to the gel phase. Laurdan spectral shifts are also dependent on the rate of relaxation of the

| (a) 440 nm | (b) 490 nm | (c) 440 nm | (d) 490 nm |
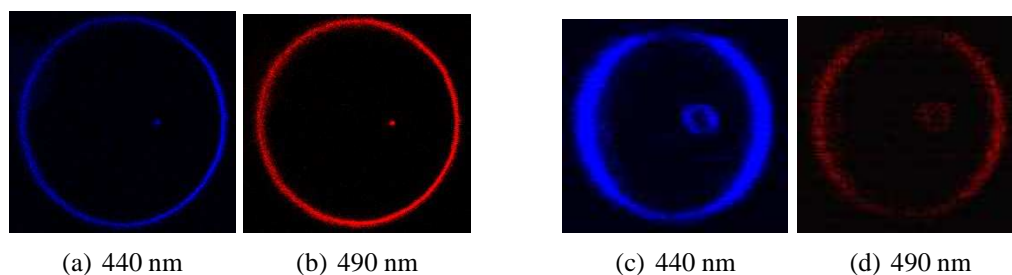
Figure 7.2: Micrographs of GUVs composed of DOPC in the fluid phase (a and b) and DPPC in the gel phase (c and d). Laurdan labeled GUV have their emission maxima at 440 nm and 490 nm in the gel and fluid phases, respectively.

solvent molecules during the relaxation of the excitation state of Laurdan. Images of Laurdan labeled GUVs are shown in Fig. 7.2 in both the fluid and gel phases. The phase state of the membrane can be obtained from the generalized polarization (GP), defined as

$$GP = \frac{I_{440} - I_{490}}{I_{440} + I_{490}} \tag{7.1}$$

where I_{440} (I_{490}) is the intensity of the blue (red shifted) emission. It is obvious from the above expression that GP lies between -1 to +1. However, in practice GP is ~ 0.2 in the fluid phase and ~ 0.8 in the gel phase. It is important to note that Laurdan is extremely sensitive to photobleaching and its life time changes from ~6 ns to ~3 ns as the membrane undergoes a transition from gel to fluid phase.

Excitation maximum of Laurdan is at about 390 nm and that of Rho PE is at 560 nm. Rho PE emits fluorescence at 580 nm and Laurdan emits at 440 nm and 490 nm, as discussed above . We have used two-photon excitation of Laurdan at a wavelength of 790 nm (Titanium Sapphire laser, power ~ 8 Watts, pulsewidth ~ 100 femtosecond). The excitation wavelength is also dependent on the solvent polarity as well as lipid phase state, therefore, optimization of excitation was performed on Laurdan labeled GUV by varying the excitation wavelength from 700 to 810 nm, keeping other setting such as detector gain and laser power fixed. Maximum intensity in the emission spectrum was obtained at an excitation wavelength of 790 nm. Due to the instant photobleaching of Laurdan labeled GUVs, it is difficult to visualize them under the microscope using mercury lamp. This problem was solved by labeling the GUVs with Rho PE also. We have observed phase separation within the GUVs by exciting
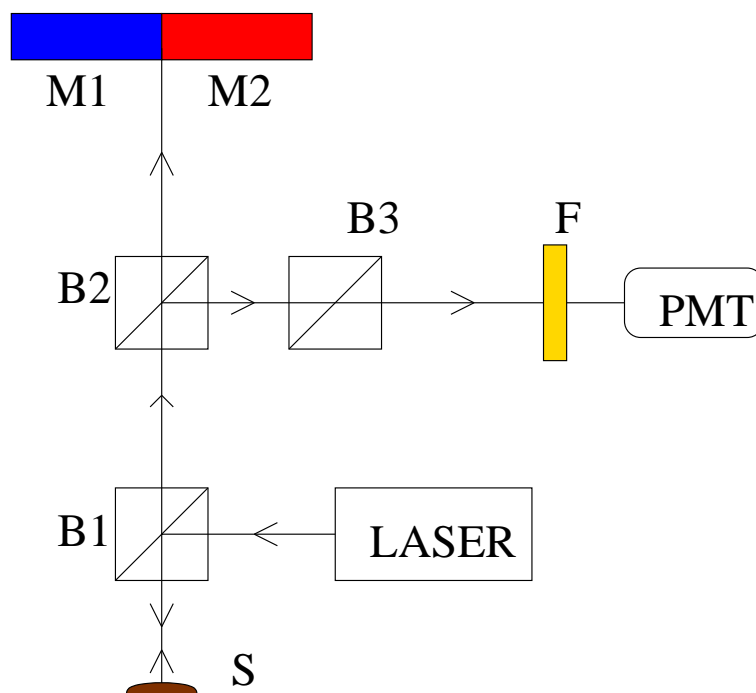
Figure 7.3: Schematic diagram of the light path used for imaging GUVs containing Rho PE as well as Laurdan. S: Specimen, B1, B2 and B3 : beam splitters, F: Filter, M1 and M2 are two selected channels in the Meta detector for Laurdan imaging having the same gain. M1 collects emitted intensity from 406 to 462 nm and M2 collects from 473 nm to 526 nm.

Rho PE, as Rho PE is known to partition preferentially into the l_d domains. A He-Ne Laser of wavelength 543 nm (1 mW) was used to excite Rho PE. Laser scanning confocal microscope (Zeiss, LSM 510) with 40X water immersion objective having a numerical aperture (NA) of 1.2 was used to obtain the images. A 63X oil immersion objective with 1.4 NA was also used. A schematic diagram of the light path in the confocal microscope is given in Fig. 7.3. The primary dichroic B1 (HFT KP 700/543) reflects both the IR laser and He-Ne laser to excite the sample. We detect Rho PE emission and Laurdan emission using a standard photomultiplier tube (PMT) and Meta detector, respectively, using a secondary beam splitter B2 (NFT KP 545). Light of wavelength (λ) larger than 545 nm (emission range of Rho PE) is selected by a long pass filter F and is collected by the PMT, whereas λ less than 545 nm are collected using the Meta detector. Therefore, the simultaneous images of Laurdan and Rho PE labeled GUVs can be obtained from the configuration described in Fig. 7.3. Pinhole aperture size were kept fixed at 283 nm for Rho PE detection. But for Laurdan detection, we

kept pinhole aperture much larger, as two-photon excitation is intrinsically confocal. Laser power and detector gain were set accordingly to optimize the emitted intensity. Typical pixel sizes of scanned images were 90 to 180 nm depending upon the selected scanned area (zoom factor).

Laser scanned GUV images were saved in 12 bit (512×512 pixels) software specified format. We collected Laurdan emission from 409-462 nm and 473-526 nm in two different channels of the Meta detector. The channels had the same gain in order to compare the relative ratio of emitted intensities at 440 nm and 490 nm.

7.4 Results and discussion

GUVs made up of binary mixtures of cholesterol with DPPC, DMPC, and ternary equimolar mixtures of a saturated lipid (DMPC, DPPC or sphigomyelin), an unsaturated lipid (DOPC) and cholesterol were investigated using laser scanning confocal fluorescence microscopy at 23°C. The polarized laser light causes photo-selection effect on Laurdan fluorescence in different phases, resulting in nonuniform intensity distribution on GUVs. Therefore, from the intensity distribution we can identify the phase state of membranes (Fig. 7.4). For example, Laurdan dipole can have all possible orientation in the fluid phase, resulting in uniform fluorescence intensity distribution on the surface of the entire GUV (Fig. 7.4 b) . However, in the gel phase molecular rotations are restricted and we observe higher intensity on the equatorial surface of GUVs, as shown in Fig. 7.4 a [13]. On the contrary, dipole of Rho PE lies perpendicular to the long molecular axis of the lipid molecule and fluorescent part of the molecule is situated above the outer surface of the membranes. Therefore, we always observe higher intensity on the polar surface of the GUVs, irrespective of the lipid phase. The fluorescence intensity distribution of Laurdan and Rho PE is illustrated in Fig. 7.5.

7.4.1 Binary mixtures

Binary mixtures of DPPC with cholesterol concentrations (X_c) of 0, 1.5, 2.5, 5, 7.5, 8.5, 10, 15, 20, 25, 30, 35 and 40 mol% were studied. All observations were performed at room
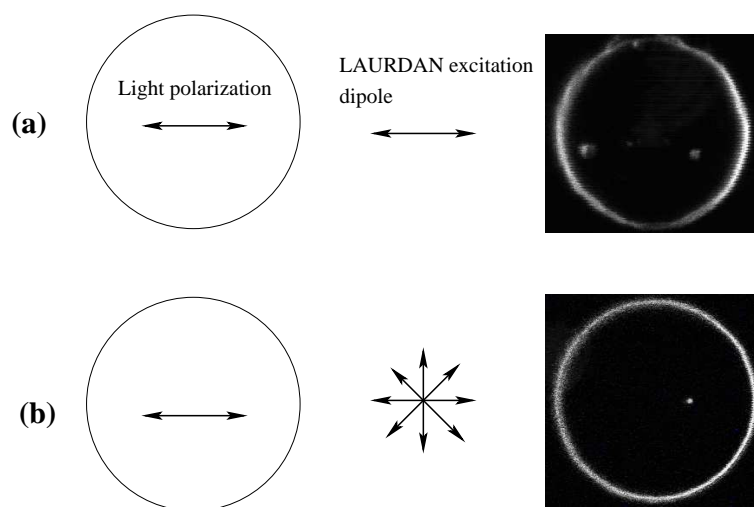
Figure 7.4: Photo-selection effect of Laurdan in the gel (a) and fluid phases (b). Arrow in the middle of the circle representing the vesicle indicates the direction of light polarization.

LAURDAN   **Rhodamine DHPE**
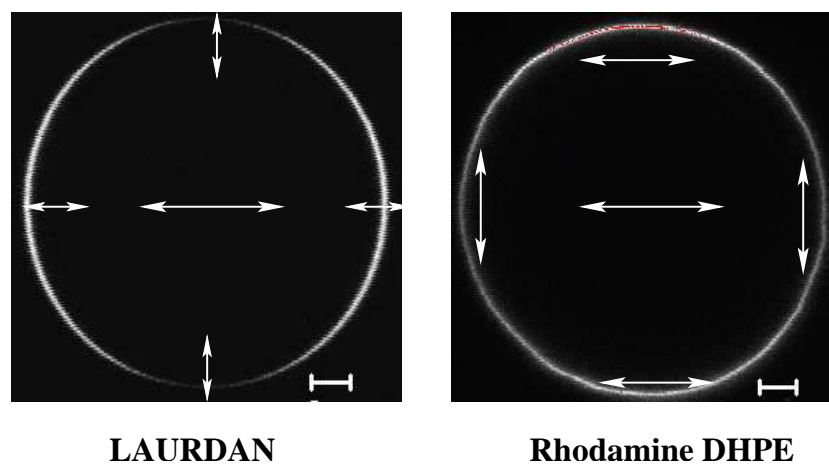
Figure 7.5: Intensity distribution of Laurdan and Rho PE labeled GUVs showing photo-selection effect in the l_o phase. Arrows in the middle of the GUVs indicate direction of light polarization and arrows on the contour represent dipole orientation of Laurdan and Rhodamine DHPE in the membranes. Scale bars, 5 μm.

temperature (23°C). Since the main- and pre-transition temperatures of DPPC are at 42°C and ~ 33°C, respectively, bilayers are in the gel phase at 23°C and we have observed a higher intensity in the blue (409-462 nm) channel than in the red shifted (473-526) channel. The value of GP in the gel phase was found to be ~ 0.8. Incorporation of small amount of cholesterol ($1.5 < X_c < 10$) changes the membrane fluidity drastically. Depending upon the size of the GUVs, we have observed different behaviour in this range of X_c.

GUVs of diameter (D) < ~ 20 μm are almost spherical in shape and exhibit phase separation. They show dark irregular domains on a bright background, indicating the coexistence of two phases (Fig 7.6). This phase separation was observed using Rho PE. Partitioning of the dye into the two phases suggests that these dark domains are in the gel phase, since Rho PE is known to prefer the fluid phase [6]. Our diffraction study on these binary mixtures have shown the coexistence of gel with the cholesterol-rich P_β phase at X_c < 10 mol% . Therefore, we would expect a similar coexistence in GUVs. This is also supported by the fact that the domains have irregular shape and do not coalesce on colliding. As the size of these dark domains are very small compared to the size of GUVs, they are clearly visible only at the top or bottom surface of GUVs (Fig. 7.6). However, we did observe significant intensity variation at the equatorial section of some GUVs due to the phase separation (Fig. 7.7). Since GUVs are not attached to the substrate, the position of the GUV was found to shift after a few scans. As a result, we were not able to obtain good three dimensional images of GUVs. The gel–fluid coexistence seen in the present study has not been observed in earlier microscopy studies [2]. It is interesting to note that number of GUVs showing the coexistence of the gel and fluid phases decreases as X_c is increased from 1.5 to 10 mol%.

For larger GUVs of D > ~ 20 μm, the coexistence of gel and cholesterol-rich phases was not observed at X_c < 10 mol% (Fig. 7.8). We have not observed domains even on the top or bottom of these GUVs, as shown in Fig. 7.8. However, we cannot rule out the possibility of phase separation, as there could be tiny gel domains which are beyond the resolution of the microscope. At these X_c, most of these GUVs show arbitrary non-spherical shapes. These non spherical GUVs exhibit pronounced thermal shape fluctuations. Interestingly, some of

(a) 1.5   (b) 2.5   (c) 5.0

(d) 7.5   (e) 8.5   (f) 10
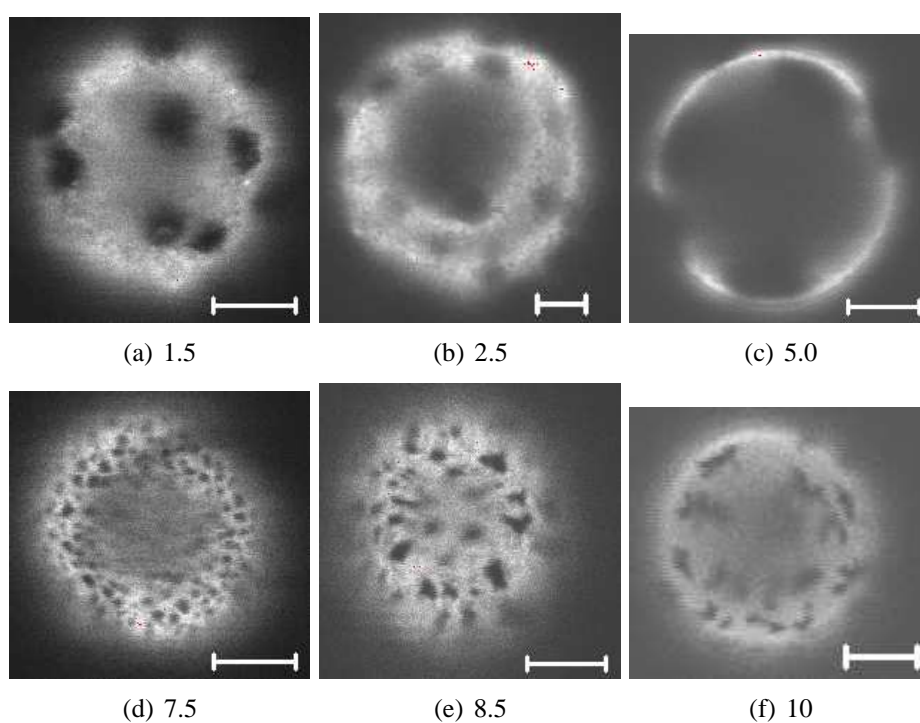
Figure 7.6: Micrographs of top surface of GUVs made from DPPC–cholesterol mixtures showing the coexistence of gel domains with the cholesterol–rich fluid phase. Cholesterol concentrations are indicated by the labels. Scale bars, 5 μm.

(a)   (b)   (c)   (d)   (e)   (f)

(g)   (h)   (i)   (j)   (k)   (l)

(m)   (n)   (o)   (p)   (q)   (r)
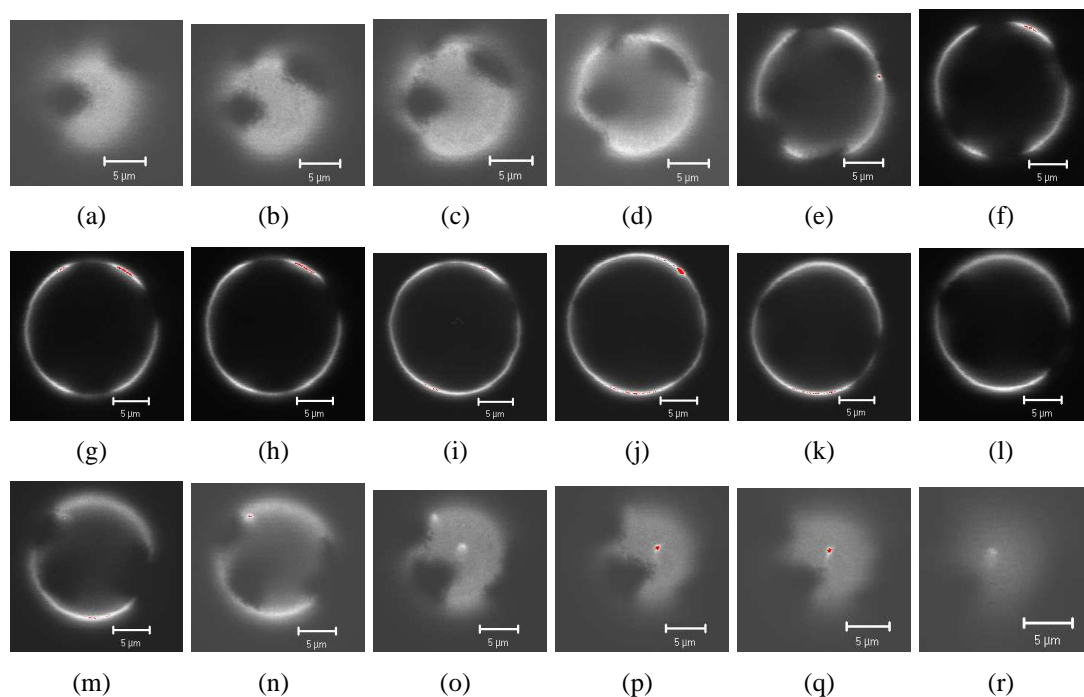
Figure 7.7: Different confocal sections from top to bottom of a GUV made from DPPC–cholesterol mixture (X_c = 5 mol%) showing coexistence of gel domains with cholesterol-rich fluid phase. Background of the top section of GUV is brighter due to change in contrast in order to make the black domains visible. Scale bars, 5 μm.
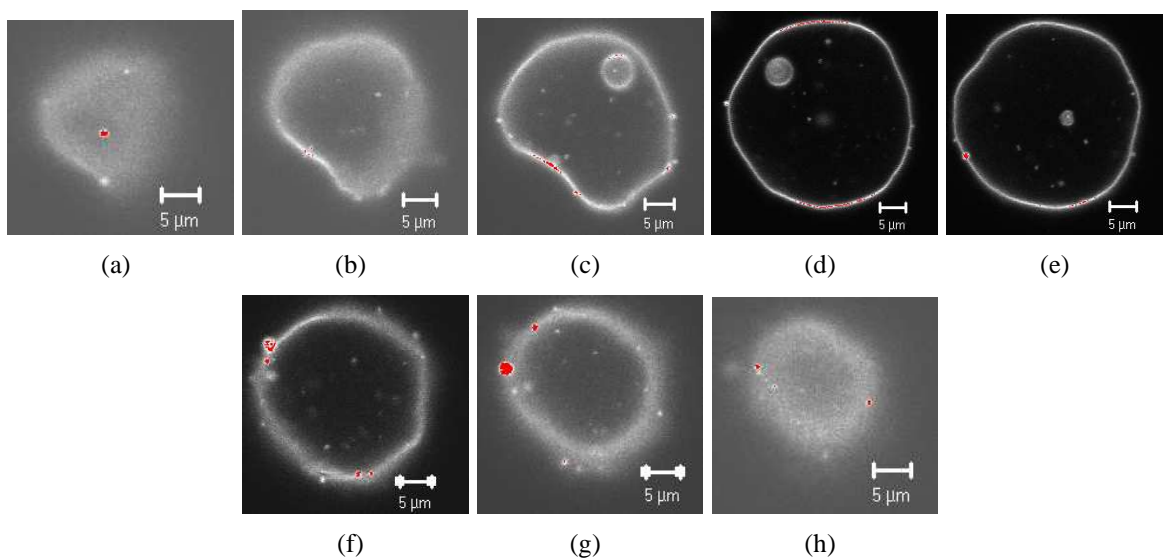
Figure 7.8: A few confocal sections from top to bottom of a GUV made up of DPPC–cholesterol mixture (X_c = 5 mol%) showing no two-phase coexistence, but exhibiting thermal shape fluctuations. Scale bars, 5 μm.

these non spherical GUVs show corrugations of their surfaces and some of them also show sharp edges, as shown in Figs. 7.9 and 7.10. As X_c is increased from 5 to 10 mol%, the number of non-spherical GUVs decreases. Many of them are quasi-spherical with corrugated surfaces. (Figs. 7.9 and 7.10).

For X_c > 10 mol%, GUVs of all sizes are almost spherical. However, these GUVs do not exhibit significant thermal shape fluctuations, indicating increase in the membrane bending rigidity with increasing X_c. GUV surface becomes smooth compared to the corrugated sur-
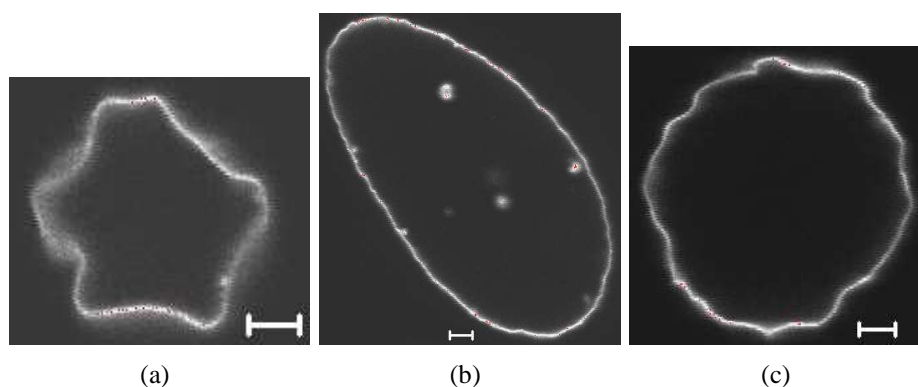
Figure 7.9: Equatorial section of GUVs made from DPPC–cholesterol mixture (X_c = 1.5 mol%), showing a variety of shapes. These GUVs also exhibit thermal shape fluctuations. Scale bars, 5 μm.
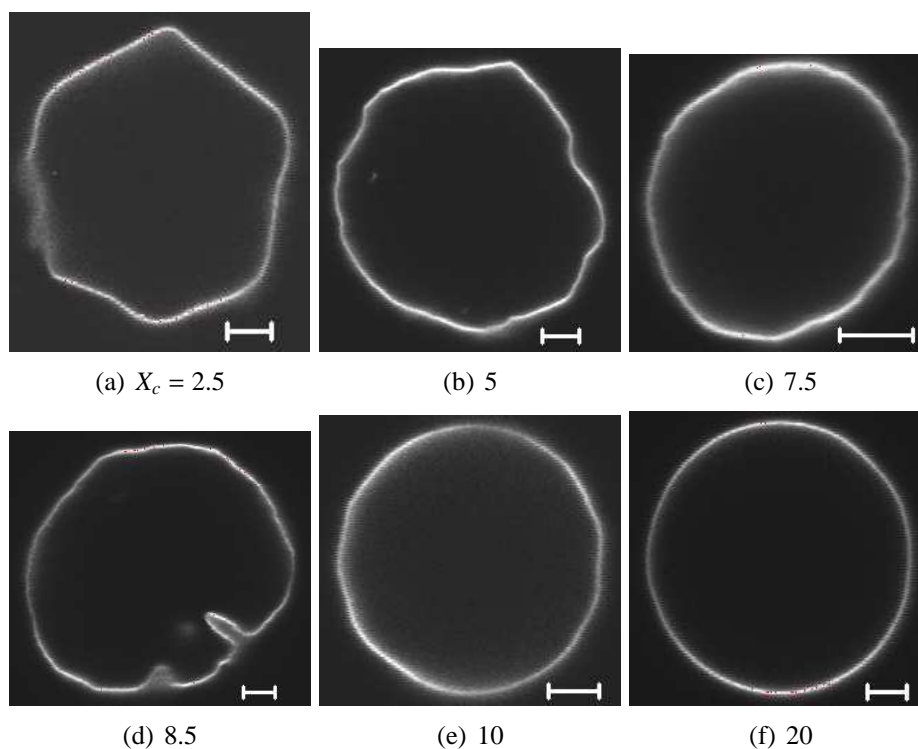
Figure 7.10: (a) Micrographs of equatorial section of GUVs composed of DPPC–cholesterol mixtures showing shape deformation. Cholesterol concentrations are indicated by the labels. GUVs exhibit thermal shape fluctuations for $X_c \leq 10$ mol%. Scale bars, 5 μm.

face observed at lower X_c. However, some GUVs show the formation of buds, as shown in Fig. 7.11 a and b. In these GUVs, some portion of the membrane has a different curvature than the rest of the GUV. Since we do not expect any phase separation at these X_c, the protrusion of the membrane might not be due to line tension. Similar behaviour was also seen in some DMPC–cholesterol GUVs (Fig. 7.11 c).

In Laurdan labeled GUVs, we have found a distribution of GP values for various GUVs at a given X_c. The variation of GP in different GUVs might be due to slight differences of X_c. However, cholesterol content of each GUV is difficult to measure. Therefore, we have calculated average Laurdan GP in order to determine the lipid phase state in the presence of cholesterol. Average GP over 20-25 GUVs at a given X_c were calculated by integrating the intensity of the entire GUVs in two different channels, as discussed above. The mean values of GP as a function of X_c are given in table 7.1. The variation of GP with X_c is shown in Fig. 7.12. It is evident from this plot that GP shows a minimum at $X_c = 2.5$ mol% and the scatter

(a) $X_c = 10$ (b) $X_c = 25$ (c) $X_c = 30$
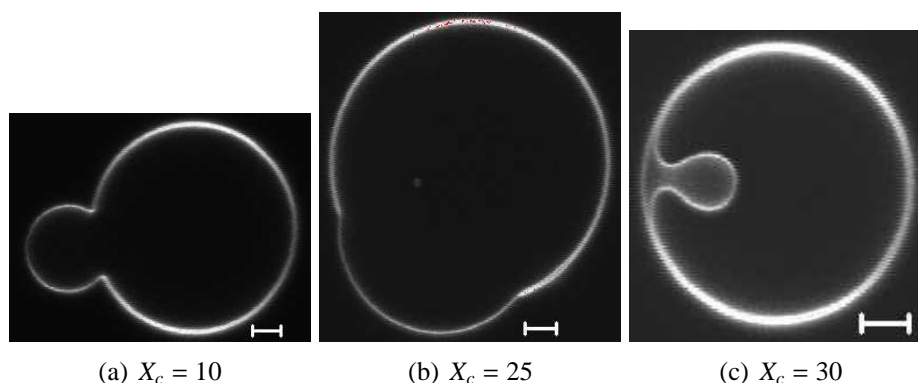
Figure 7.11: Equatorial section of GUVs made from DPPC–cholesterol mixtures (a and b) and DMPC–cholesterol mixture (c) showing bud like structure. Scale bars, 5 μm.

is much higher for lower values of X_c. This could be the consequence of the fact that at these X_c, larger GUVs show thermal shape fluctuations, indicating the increase in the fluidity of the membranes in the presence of cholesterol. GUVs that show low GP also show uniform intensity distribution on their surfaces, indicating fluid membranes. In the measurement of GP we have not separated the bigger GUVs from the smaller ones. The large scatter in GP at low X_c is almost certainly due to the difference in the behaviour of the GUVs depending on their size, described above. At higher X_c, GP remains constant at ~ 0.8 which is the typical value found in the gel phase, due to the lower water penetration into the membranes [14]. This could be the result of denser packing of the molecules in this phase which also leads to a higher rigidity of membranes and lower mobility of molecules. The fact that the scatter in GP is small at higher X_c indicates that all of them are in similar phase state. This phase was identified as the liquid ordered phase in our diffraction study. The higher intensity on the equatorial surface of these GUVs indicates that this phase is more ordered than the one occurring at lower X_c.

Smaller GUVs of D < 20 μm exhibit phase separation irrespective of their shape. The fact that larger GUVs do not show domains might be the consequence of differences in the kinetics of the nucleation process involved in the formation of domains. This could be due to the fact that the smaller GUVs are more tense than larger ones. Occurrence of sharp edges in non-spherical large GUVs in the absence of any phase separation is intriguing,

Table 7.1: Generalized polarization (GP) values of Laurdan in GUVs composed of DPPC at different cholesterol concentrations.

X_c (mol%)	GP	X_c (mol%)	GP
0.0	0.81 ± 0.05	10.0	0.73 ± 0.08
1.5	0.70 ± 0.08	15.0	0.64 ± 0.10
2.5	0.42 ± 0.20	20.0	0.70 ± 0.03
5.0	0.77 ± 0.12	25.0	0.76 ± 0.06
7.5	0.77 ± 0.13	30.0	0.77 ± 0.06
8.5	0.84 ± 0.04	35.0	0.72 ± 0.04

$$GP = \frac{I_{440} - I_{490}}{I_{440} + I_{490}}$$
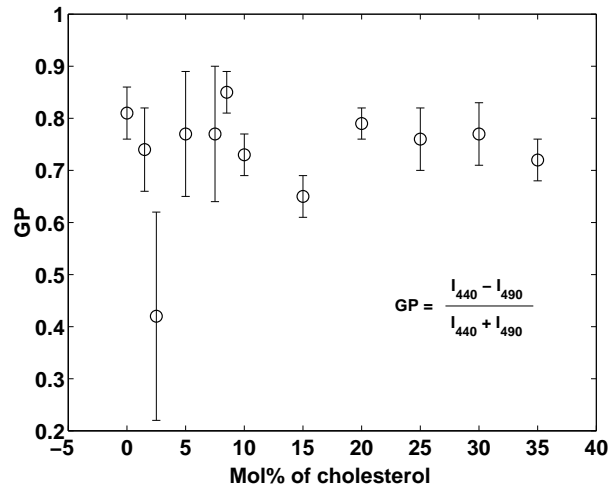
Figure 7.12: Mean values of GP obtained from GUVs made up of DPPC–cholesterol mixtures. Error bars show a standard deviation from the mean.

since the formation of such structure is normally associated with the presence of domains with sufficiently different membranes properties. The significant thermal shape fluctuations of these GUVs for $X_c < 5$ mol%, at lower temperature is also surprising, as cholesterol is expected to increase the bending rigidity of the membranes compared to that in the fluid (L_α) phase observed above T_m. At these X_c, a plot of Laurdan GP as a function of X_c also shows a dip, indicating flexible membranes (Fig 7.12). Thermal shape fluctuations at low X_c imply the softening of bilayer. The low GP of DPPC–cholesterol mixture ($X_c = 5$, GP =0.52 ±0.13) at 20°C, compared to the value at room temperature (25°C, GP = 0.77 ±0.12) implies that bilayer becomes more soft at lower temperatures. The softening of bilayer is consistent with the large d-spacing of the cholesterol induced modulated (P_β) phase found in the diffraction

(a)   (b)   (c)

(d)   (e)   (f)
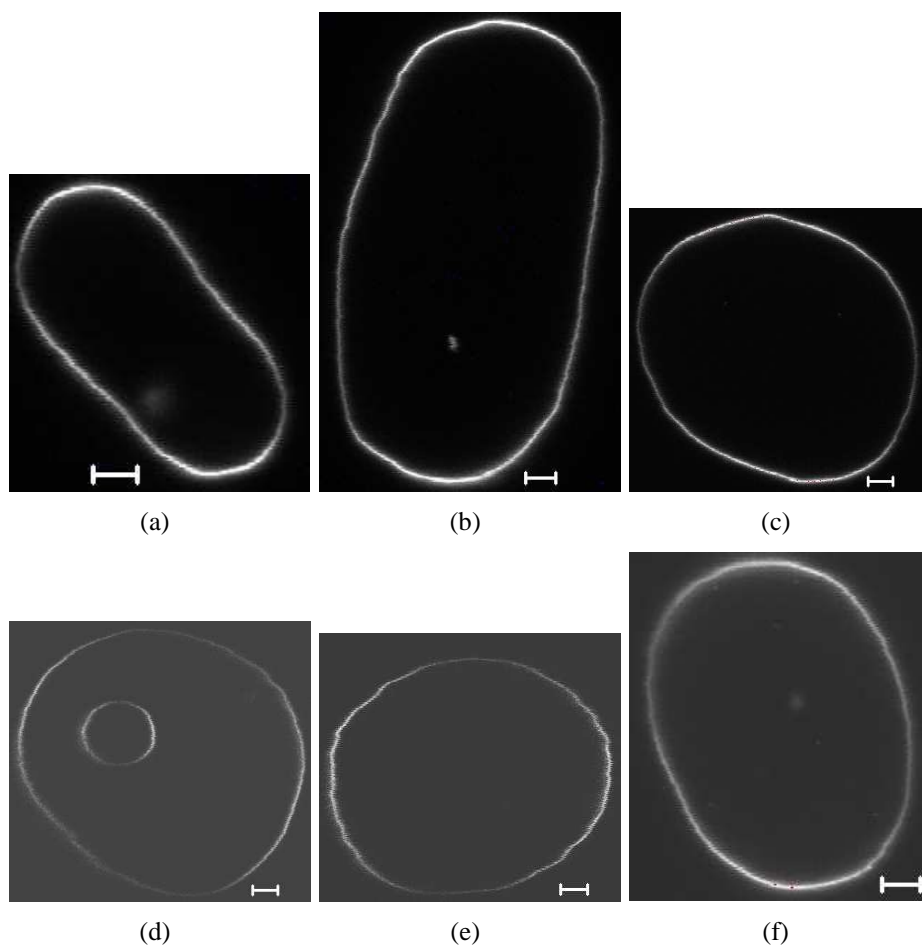
Figure 7.13: Deviation from a spherical shape found in DMPC–cholesterol mixtures. Equatorial section of GUVs shown in a, b, c were obtained at $X_c = 10$ mol% and d, e, f at $X_c = 20$ mol% (T = 23°C). Scale bars, 5 μm.

experiments at similar values of X_c.

In order to understand the origin of the shape change and thermal shape fluctuations observed in GUVs made from DPPC–cholesterol mixtures, we have carried out similar experiments with DMPC–cholesterol mixtures. These experiments were done at temperature ~ T_m of the DMPC. Hence we could not probe the gel–L_α phase separation. Unlike the GUVs made from DPPC–cholesterol mixtures, behaviour of these GUVs, irrespective of their size is found to be similar. It is an interesting observation that GUVs of DMPC and DMPC cholesterol mixtures do not exhibit significant thermal shape fluctuations and most of the GUVs are almost spherical in shape at low values of X_c (< 10). For $10 \leq X_c <25$, most of the GUVs are non-spherical in shape, as shown in Fig. 7.13. However, at $X_c > 25$ mol%, GUVs are spher-

ical in shape. Since GUVs, made up of these mixtures do not exhibit pronounced thermal shape fluctuations, the shape deformation observed in DMPC–cholesterol mixtures might have a different origin from those observed in DPPC–cholesterol mixtures. This observation may be related to the fact that DPPC-cholesterol mixtures exhibit P_β phase at room temperature, whereas this phase occurs at much lower temperatures ($< 13°C$) in DMPC–cholesterol mixtures. The non spherical shapes seen in DMPC–cholesterol GUVs (Fig. 7.13) resemble those observed by Käs et al. in DMPC on increasing the temperature [3]. These have been explained as arising from changes in the excess area of the membrane and from asymmetric thermal expansivity of monolayers. The shape deformation of multicomponent membranes can arise from the minimization of line tension between two coexisting phases. It has been suggested by Seifert that budding in two component spherical vesicles can take place even in the absence of phase separation if there is an asymmetry in the density of the two monolayers. Therefore, even in the absence of phase separation, the coupling of density in the two monolayer with curvature can in principle lead to a shape deformation such as that shown in Fig. 7.11 [4, 5]. It is also possible that the softening of the bilayer at lower X_c is a result of the coupling between curvature and fluctuations in the concentration. Such a coupling can in principle reduce the bending rigidity of the membranes. Further experimental work as well as theoretical studies are required to understand this behaviour better.

7.4.2 Ternary mixtures

We have studied equimolar mixtures of three ternary systems (DMPC/DOPC/cholesterol, DPPC/DOPC/cholesterol and sphigomyelin/DOPC/cholesterol) which are known to be raft forming compositions. These experiments were done at room temperature ($23°C$). All three mixtures show black circular domains on a bright background (Fig. 7.14). Partitioning of Rho PE in the two phases implies that the black domains are the more ordered phase, coexisting with the disordered fluid phase. Since GUVs are formed at high temperatures (above T_m), they do not show domains immediately after the transfer to the cover slip for observation. These fluid domains appear when the aqueous solution containing GUVs attains
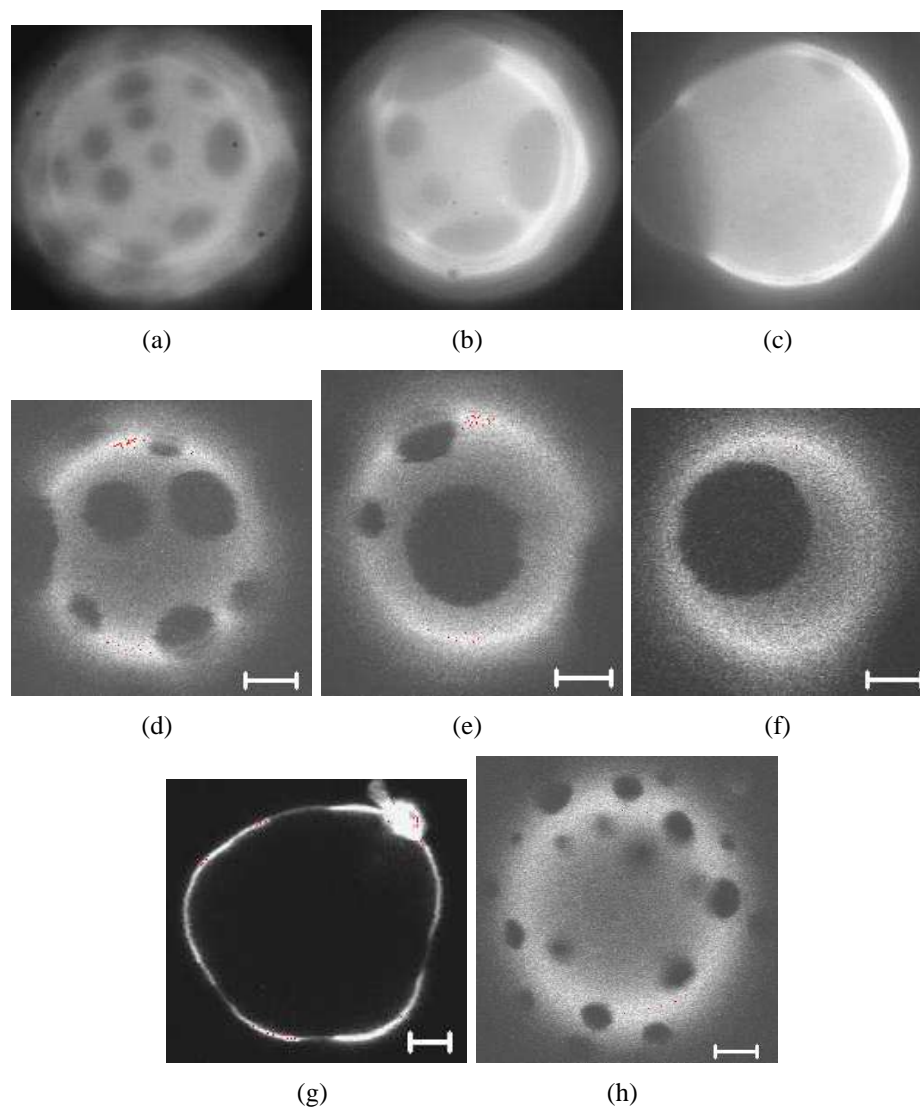
Figure 7.14: Micrographs of GUVs made from equimolar ternary mixtures of cholesterol and DOPC with DMPC (a, b, c), with DPPC (d, e, f) and with sphingomyelin (g). (h) is obtained from a DPPC–DOPC–DHE mixture. The set of three images of GUVs (a, b, c) were taken with a CCD camera using a conventional fluorescence microscope with 40X objective. Size of these vesicles is $\sim 40\,\mu$m. (d), (e), (f) and (h) are the top section and (g) is the equatorial section of GUVs obtained using laser scanning confocal microscopy. These GUVs show the coexistence of two fluid phases. Growing fluid domains eventually form a bigger domains over a time scale of ~ 1 minute, as depicted in (a, b, c) and (d, e, f). Scale bars, 5 μm.

room temperature. The fact that these domains are circular in shape and are also mobile indicates that they are in a fluid phase. Smaller circular domains on GUVs grow with time and coalesce on colliding and eventually form bigger domains over a time scale of the order of a minute, as shown in Fig. 7.14. Final size of these domains is ∼ 10 μm. These results are in agreement with earlier observations using fluorescence microscopy [2, 6].

It is interesting to note that small domains do not form buds, only the bigger domains do. The domain induced budding of these GUVs has been explained theoretically taking into account the line energy at the boundary of two coexisting phases and the bending energy of individual domains. The bud size is found to depend on the rigidity of the growing domains [15]. It was suggested by Jülicher and Lipowsky that the shape of these GUVs and the budding of domains depend on the kinetics of phase separation even if pressure difference between the inside and the outside of the GUV is zero. The phase separation between two fluid phases via spinodal decomposition was discussed in ref. [2]. Sufficiently large spontaneous curvature of the membrane in the domains can also in principle lead to budding in case of vanishing line tension. As can be seen from the Fig. 7.14 c, black domains bulge out and form a bud, whereas Fig. 7.14 g shows protrusions of bright regions. Thus both phases are capable of forming buds. This is consistent with an earlier two-photon fluorescence microscopy study on this system [6]. It was shown that both phases can bud, with no curvature preference for these two coexisting phases, indicating that the line tension is important for the budding process. Baumgart et al. have estimated the typical line tension from the shape analysis of two coexisting domains and it is found to be $9 \pm 0.3 \times 10^{-13}$ N [6].

Coexistence of two fluid phases seen in fluorescence microscopy is in broad agreement with the results of x-ray diffraction studies discussed in chapter 6. Since we have observed the DPPC–rich l_o and the DOPC–rich l_d phases in our diffraction study, we expect a similar coexistence in GUVs.

As discussed in chapter 3, dehydroergosterol (DHE) is a fluorescence analog of cholesterol. We have studied an equimolar mixture of DPPC, DOPC and DHE doped with 0.2 mol% of Rho PE. Domains have been observed in this system, similar to that observed using

cholesterol (Fig. 7.14 h). DHE is fluorescent and can be excited at ~ 300 nm. Therefore, in principle it can be used as a pertinent probe to measure the cholesterol distribution quantitatively in the two fluid phases. Although DHE can be excited using three-photon excitation, we were not able to obtain good signal to noise ratio from DHE with our present setup. Therefore, we have not been able to determine the partitioning of DHE into the two coexisting phases.

7.5 Conclusion

Confocal fluorescence microscopy studies on GUVs support the results of diffraction experiments on binary and ternary systems discussed in previous chapters. Domains were observed in GUVs made from both binary and ternary mixtures. But there is an important difference in the nature of the domains in the two systems; in the ternary mixtures they are in the fluid phase, whereas in the binary mixtures they are in the gel phase. Domains in binary mixtures have not been observed in earlier microscopy experiments on GUVs. Shape deformation and thermal shape fluctuations at low X_c in DPPC–cholesterol mixtures are interesting and distinct from the shape changes observed earlier in the vicinity of the main transition. This feature of GUVs at low X_c has been so far overlooked in the literature. Softening of the bilayer at low X_c could be due to the occurrence of the cholesterol induced modulated (P_β) phase where bilayers are more flexible, as indicated by diffraction experiments. However, spherical rigid GUVs were observed at $X_c > 15$. Further studies are required to understand these shape deformations and thermal shape fluctuations observed in the absence of any phase separation.

Bibliography

[1] L. A. Bagatolli and E. Gratton, Biophys. J. **77**, 2090 (1999).

[2] S. L. Veatch and S. L. Keller, Phys. Rev. Lett. **89**, 268101 (2002) ; Biophys. J. **85**, 3074 (2003).

[3] J. Käs and E. Sackmann, Biophys. J. **60**, 825 (1991).

[4] R. Lipowsky and E. Sackmann, ed. *Handbook of Biological Physics* (Elsevier Science B. V, 1995).

[5] U. Seifert, Phys . Rev. Lett. **70**, 1335 (1993) ; Adv. Phys. **46**, 13 (1997).

[6] T. Baumgart, S. T. Hess, and W. W. Webb, Nature **425**, 821 (2003).

[7] C. Dietrich, L. A. Bagatolli, Z. N. Volovyk, N. L. Thompson, M. Levi, K. Jacobson, and E. Gratton, Biophys. J. **80**, 1417 (2001).

[8] D. Scherfeld, N. Kahya, and P. Schwille, Biophys. J. **85**, 3758 (2003).

[9] M. Laradji and P. B. S. Kumar, Phys. Rev. Lett. **93**, 198105 (2004).

[10] M. I. Angelova, S. Soléau, Ph. Méléard, J. F. Faucon, and P. Bothorel, Progr. Colloid. Polym. Sci. **89**, 127 (1992).

[11] T. Parasassi, E. Gratton, W. M. Yu, P. Wilson, and M. Levi, Biophys. J. **72**, 2413 (1997).

[12] L. A. Bagatolli, T. Parasassi, G. D. Fidelio, and E. Gratton, Photochem Photobiol. **70**, 557 (1999).

[13] L. A. Bagatolli and E. Gratton, Biophys. J. **78**, 290 (2000).

[14] T. Parasassi, M. D. Stefano, M. Loiero, G. Ravagnan, and E. Gratton, Biophys. J. **66**, 120 (1994).

[15] F. Jülicher and R. Lipowsky, Phys. Rev. Lett. **70**, 2964 (1993).